Title

Multiscale, multispectral fluorescence lifetime imaging using a double-clad fiber.

Journal

Optics Letters, 44(9)

ISSN

0146-9592

Authors

Sherlock, Benjamin E

Li, Cai

Zhou, Xiangnan

et al.

Publication Date

2019-05-01

DOI

10.1364/ol.44.002302

Peer reviewed

HHS Public Access

Author manuscript

Opt Lett. Author manuscript; available in PMC 2020 October 07.

Published in final edited form as:

Opt Lett. 2019 May 01; 44(9): 2302–2305. doi:10.1364/OL.44.002302.

Multiscale, multispectral fluorescence lifetime imaging using a double-clad fiber

Benjamin E. Sherlock[1,3], **Cai Li**[1], **Xiangnan Zhou**[1], **Alba Alfonso-Garcia**[1], **Julien Bec**[1], **Diego Yankelevich**[1,2], **Laura Marcu**[1,*]

[1]Genome and Biomedical Sciences Facility, University of California, Davis, 451 Health Sciences Drive, Davis, California 95616, USA

[2]Department of Electrical and Computer Engineering, University of California, Davis, One Shields Avenue, Davis, California 95616, USA

[3]bsherlock@ucdavis.edu

Abstract

Fiber-based imaging of tissue autofluorescence using ultraviolet (UV) excitation is a highly flexible tool used to probe structure and composition. In this Letter, we report, to the best of our knowledge, the first results from a single-fiber imaging system employing a custom double-clad fiber to acquire multispectral fluorescence lifetime images at two distinct spatial resolutions. We characterize the lateral point spread function and fluorescent background of the system and show how enhanced resolution can identify features such as trabeculae in *ex vivo* murine bone samples.

Fluorescence imaging of unlabeled biological tissues using ultraviolet (UV) light is a powerful tool for investigating tissue structure and composition [1]. The low penetration depth of light in tissue has motivated the development of fiber-based imaging systems, wherein light is guided to and from the tissue of interest inside one or more optical fibers [2–4]. Fiber-based imaging systems employing separate fibers for light delivery and collection are able to probe the fluorescent and optical properties of tissue at different depths while being relatively insensitive to fiber autofluorescence. However, some applications, e.g., imaging the luminal surface of the coronary arteries, present such restricted geometries that only a single-fiber optic can be accommodated. For these single-fiber applications, image data are most commonly acquired by mechanically scanning the fiber output across the sample surface.

Silica multimode fibers (MMFs) are frequently used in fiber-based fluorescence imaging systems. MMFs guide UV light with low attenuation and background autofluorescence. Furthermore, they possess aperture sizes and numerical apertures (NAs) which are compatible with capturing sufficient backscattered sample autofluorescence to achieve good image quality. One disadvantage of MMFs is that they lack a simple way to change the geometric extent of the point spread function (PSF) in the image plane. Fiber-based fluorescence imaging is often performed at the tissue level, where millimeter-sized fields of

*Corresponding author: lmarcu@ucdavis.edu.

view must be imaged in <1 min. However, it is also desirable to investigate features of interest identified in the initial image at a higher resolution. Fiber-based imaging applications such as compositional assessments of atherosclerotic plaques [5], intraoperative margin assessment during tumor resection [6], vascular stent endothelization, and longitudinal monitoring of cellular proliferation in engineered tissue constructs [7] would benefit from the flexibility to quickly and simply change the resolution.

Pioneering work is currently underway to demonstrate focusing and scanning of light through a MMF [8], though considerable challenges remain before the promise of this field can be brought to bear in a clinical environment. Multicore fibers offer several intriguing possibilities for fluorescence imaging; however, the most commonly used fibers (e.g., Fujikura FIGH-100-1500N) exhibit strong autofluorescence, postulated to originate from fiber dopants such as Germanium, when guiding UV light [9].

Double-clad fibers (DCFs) possess two concentric regions that are compatible with optical guidance. A small central core is surrounded by a larger multimode cladding. Recently, it has been shown that the core and cladding regions of a DCF can support different imaging modalities [10–12]. By switching illumination between the cladding and core of a DCF, multiscale fiber-coupled fluorescence imaging is achieved. However, the glass dopants used to realize a conventional DCF core interact strongly with UV light, causing high background fluorescence and UV attenuation [13]. Thus, conventional DCFs do not support multiscale fluorescence imaging using UV excitation. In 2016, a double-clad photonic crystal fiber was fabricated and used for fluorescence spectroscopy and lifetime measurements using 405 nm excitation [14].

Here we report, to the best of our knowledge, the first results from the integration of a DCF compatible with guiding UV light in both the core and cladding regions at low attenuation and background, with our fiber-based fluorescence lifetime imaging (FLIm) system. The DCF enables multispectral fluorescence lifetime images to be acquired at two distinct spatial resolutions. We characterize the transmission, autofluorescence background, and lateral PSF of the DCF core and cladding regions. Finally we show images of sample autofluorescence acquired using the core and cladding guided 355 nm pulsed laser light.

A custom-made DCF was developed for this Letter. The DCF consists of three concentric regions of pure and fluorine-doped silica. A 10 μm diameter pure silica core, surrounded by a region of fluorine-doped silica can be used to guide UV light to the sample, when high-resolution fluorescence images are required. UV light can also be injected into a 600 μm diameter pure silica outer cladding which provides imaging resolution similar to a MMF. A low-index polymer jacket satisfies the condition for total internal reflection of light above the critical angle in the outer cladding.

All results presented here were acquired using our fiber-based multispectral FLIm system (see Fig. 1) which has been reported in detail previously [12]. Briefly, the output of a frequency-tripled, Nd:YAG microchip *Q*-switched laser (355 nm, 0.6 ns pulses, 4 kHz repetition rate, 7.89 mW average power output), was coupled into a 4 m long section of the custom-made DCF patch cord. The patch cord is connectorized at either end by a custom-

made fiber-optic connector angled physical contact ferrules. A kinematic mirror is used to introduce minor and repeatable adjustments to the angle of the UV light at the fiber coupling lens back focal plane. By controlling the position of the fiber coupling lens focus, UV light is selectively injected into either the DCF core or cladding. The effective NA of the core and cladding regions was measured to be 0.08 and 0.22, respectively. These values represent lower bounds for the NA, as we underfill the fiber NA at the input side and, thus, not all guided modes are populated. The transmission of the DCF core and cladding at 355 nm was measured to 0.33 and 0.55, respectively.

At the distal end of the fiber, a 1.8 mm diameter, 11 mm long lithium ion exchange gradient index (GRIN) lens (NA = 0.2, GT-LFRL-180-025-20-NC, GRINtech) is mounted to the fiber ferrule using a ceramic split sleeve connector. The GRIN lens images the distal end face of the fiber onto the sample surface at approximately unity magnification. Backscattered sample autofluorescence is guided by all regions of the DCF to a four-channel wavelength selection module (WSM) realized by four dichroic beam splitters and spectral filters. The spectral distribution of the WSM fluorescence detection channels is as follows: CH1 = 390/18 nm, CH2 = 435/40 nm, CH3 = 543/21 nm, and CH4 = 610/70 nm. Each channel of the WSM is temporally multiplexed onto a single multichannel plate photomultiplier tube (MCP-PMT) using four fiber optic delay lines. The MCP-PMT output is amplified before being recorded by a National Instruments data acquisition card (DAQ) operating at 12.5 GS/s.

Fluorescence decays are acquired using the pulse sampling technique. The instrument response function is recorded at the start of each imaging session. Fluorescence lifetimes are extracted from the raw decays using a constrained least-squares deconvolution with the Laguerre expansion technique [15]. Fluorescence images are constructed in a pointwise manner, analogous to laser scanning microscopy, by raster scanning the GRIN lens and fiber tip assembly over the sample surface using a motorized three-axis translation stage. The stage was programmed to use the step sizes of 10 μm/pixel under core illumination and 100 μm/pixel under cladding illumination. To improve the image signal-to-noise ratio (SNR), 16 fluorescence decays were recorded and averaged for each pixel. A realtime algorithm that rapidly adjusted the bias voltage on the MCP-PMT to enhance the dynamic range of the detector further reduced the effective pixel acquisition rate to 78 Hz [16].

In Fig. 2(a), we present time-resolved fluorescence intensity traces recorded in CH1. The traces compare the amplified MCP-PMT output when using a MMF, DCF core, or DCF cladding to guide pulsed UV light. The main traces were acquired in the absence of a sample and show only fiber background. The inset plot shows traces recorded when the DCF was used to illuminate a section of murine bone (see Fig. 4). Three distinct regions of the traces can be identified. From 0 to 10 ns, the laser pulse propagates in air, and no background fluorescence is observed. From 10 to 30 ns, the pulse propagates inside the fiber, causing a low constant background fluorescence to be detected. From 30 ns onwards, the trace reports fluorescence generated as the pulse exits the fiber. In the main plot, we understand the fluorescence generated in the absence of a sample to result from UV light scattering at the fiber tip and exciting fluorescence in the fiber jacket. This stable background signal is recorded prior to each measurement and subtracted during data processing. A 13 μm

tungsten wire coated with a thin layer of fluorescent dye was used to estimate upper bounds for the lateral extent of the core and cladding PSF [Fig. 2(b)]. The focal plane of the DCF core was located 2.75 mm from the distal end of the GRIN lens, and the lateral PSF was measured to be 28.2 ± 1.9 μm. Interestingly, the cladding region focal plane was located 4.5 mm from the GRIN lens distal tip. The lateral PSF of the cladding region was measured to be 250 ± 3.2 μm, a value which is similar to what we have previously reported for MMFs of similar dimensions [17]. We postulate that the presence of strong spherical aberrations in the GRIN lens is the cause of the offset between the core and cladding focal planes, as light from each fiber region propagates through radially different regions of the lens. The separation between the fiber tip assembly and sample surface was adjusted using the vertical axis of the translation stage when switching between the core and cladding illumination to compensate for the focal plane offset.

The DCF should recover the same lifetime from a known fluorescent dye, regardless of the region of the fiber used for illumination. In Table 1, we report the mean fluorescence lifetimes recorded for Coumarin 1 (in EtOH) and Rhodamine B (in EtOH) in the fluorescence detection channel where the dye fluorescence emission peaks (CH2 and CH4, respectively, for this apparatus). The recorded lifetimes agree both with each other and with literature quoted values [18,19] and, thus, indicate that both regions of the DCF are compatible with making reliable lifetime measurements.

In Figs. 3–5, we report images that display the resolution enhancement afforded by DCF core illumination. We note here that when imaging using the DCF core, the image acquisition time is dramatically increased in comparison with cladding illumination.

For example, the 5 by 2 mm^2 images in Fig. 3 took 30 s to acquire using cladding illumination and 29 min using core illumination. We emphasize that our intention is not to use DCF core illumination to routinely image millimeter scale regions, but rather to use DCF cladding illumination to identify subregions of interest, and then investigate these regions at higher resolution using core illumination. Images of laser-printed characters on white paper are presented in Fig. 3. The fluorescence intensity image (CH2) acquired using core illumination shows excellent agreement with a photograph of the printed characters and highlights the improved lateral resolution and contrast recovery with respect to the cladding illumination image. Multispectral intensity-weighted fluorescence lifetime images from a 5 by 5 mm^2 section of murine long bone are reported in the Fig. 4. The same field of view was imaged using both cladding (top row) and core (bottom row) illumination. The core illumination allows for straightforward visual identification of the trabeculae. The mean fluorescence lifetimes in the core and cladding images show excellent agreement. The final sample to be imaged was a 10 by 20 mm^2 section of bovine muscle, which presents a variety of tissues (myofibers, connective, adipose). In Fig. 5 (top row), we show intensity-weighted lifetime images acquired in CH2 using MMF, DCF cladding, and DCF core illumination, along with a high-resolution image of sample autofluorescence intensity acquired using a conventional fluorescence microscope (Keyence fluorescence microscope, 4X objective). The lifetime images show strong contrast between the shorter lifetimes of the protein-rich regions and the longer lifetimes of the lipid-rich regions. The zoomed-in images (Fig. 5, bottom row) show the enhanced detail recorded in the core illumination images.

The reduction of the beam cross section enabled by core illumination significantly increases the UV irradiance of the sample, potentially limiting its clinical translation. The American National Standard for Safe Use of Lasers (ANSI Z136.1) specifies safe values of maximum permissible exposure (MPE) of tissue. Following these guidelines, the laser pulse energy for cladding and core illumination should be 5.5 and 0.017 uJ, respectively. The cladding excitation pulse energy of 0.85 μJ, therefore, is safe, whereas the core pulse energy of 0.53 μJ is noncompliant. To address this, we compared the SNR acquired in CH2 from the fluorescence emission of white card, using core illumination with the average powers of 2.12 and 0.15 mW (data not shown). In this case, the pulse energy of 0.038 μJ is only 2.23 times the MPE threshold.

The SNR for one pixel was calculated for the high and low powers as 39.6 and 38.4 dB, respectively. The small reduction in the SNR following a 93% reduction in core pulse energy suggests that compromises to remain within MPE limits when using core guided illumination will be possible for future *in vivo* imaging applications. Furthermore, high NA GRIN micro-objectives could be used to capture a larger fraction of fluorescence. Underfilling the back aperture of these micro-objectives would allow a greater fraction of fluorescence to be detected without increasing the irradiance.

In conclusion, we have presented, to the best of our knowledge, the first results from a fiber-based, multiscale, multispectral FLIm system. A specialized DCF has enabled the delivery of 355 nm fluorescence excitation to the sample surface via either a 10 μm diameter central core or 600 μm diameter cladding. A simple adjustment in the optical alignment allows switching between the DCF region used for UV light guidance and, thus, the image resolution. We have shown that both DCF regions recover similar fluorescence lifetimes from standard fluorescent dyes. Our apparatus employs a simple GRIN lens-based probe to image the distal tip of the fiber onto the sample surface. Two biological samples have been imaged to show how the enhanced resolution afforded by confining fluorescence excitation light to the DCF core can be used to identify features at the sample surface that are not resolved under cladding illumination.

We anticipate that the capability to switch the resolution of a single-fiber UV fluorescence imaging system will provide critical new insight in future studies. A fiber-based FLIm system is currently used intraoperatively to assess tumor margins during robotic surgery [6]. The ability to investigate suspected positive margins at higher spatial resolution will have a significant impact on the sensitivity and specificity of this measurement. Resolution enhancement would also benefit fiber-based fluorescence imaging studies taking place in the intravascular environment. For example, sub-100 μm^2 regions of macrophage infiltration in the fibrous cap of an atherosclerotic plaque could be detected and accurately quantified. Furthermore, an assessment of endothelial cell confluency in recellularized engineered vascular tissue [20] would be improved by the ability to detect small defects in the endothelium. Finally, although the tissue irradiance increases dramatically with the reduction in beam size, our measurements suggest the overall excitation pulse energy can be accordingly reduced to comply with optical exposure limits.

Acknowledgment.

The authors gratefully acknowledge the support from Coherent Inc. (Salem, NH) who manufactured the DCF used in this Letter.

Funding. National Institutes of Health (NIH) (1R01HL121068-01A1); California Institute for Regenerative Medicine (CIRM) (RT3-07879, RT3-07981).

REFERENCES

1. Croce AC and Bottiroli G, Eur. J. Histochem 58, 2461 (2014). [PubMed: 25578980]
2. Raman RN, Pivetti C, and Matthews D, Opt. Express 17, 894 (2009). [PubMed: 19158904]
3. Thomas P, Pande P, Clubb F, Adame J, and Jo JA, Photochem. Photobiol 86, 727 (2010). [PubMed: 20331523]
4. Nie Z, An R, Hayward JE, Farrell TJ, and Fang Q, J. Biomed. Opt 18, 096001 (2013). [PubMed: 24002188]
5. Bec J, Phipps JE, Gorpas D, Ma D, Fatakdawala H, Margulies KB, Southard JA, and Marcu L, Sci. Rep 7, 1 (2017). [PubMed: 28127051]
6. Gorpas D, Phipps J, Bec J, Ma D, Dochow S, Yankelevich D, Sorger J, Popp J, Bewley A, Gandour-Edwards R, Marcu L, and Farwell DG, Sci. Rep 9, 1187 (2019). [PubMed: 30718542]
7. Hofmann MC, Whited BM, Criswell T, Rylander MN, Rylander CG, Soker S, Wang G, and Xu Y, Tissue Eng. Part C Methods 18, 677 (2012). [PubMed: 22439610]
8. Choi Y, Yoon C, Kim M, Yang TD, Fang-Yen C, Dasari RR, Lee KJ, and Choi W, Phys. Rev. Lett 109, 203901 (2012). [PubMed: 23215488]
9. Udovich JA, Kirkpatrick ND, Kano A, Tanbakuchi A, Utzinger U, and Gmitro AF, Appl. Opt 47, 4560 (2008). [PubMed: 18758526]
10. Ryu SY, Choi HY, Na J, Choi ES, and Lee BH, Opt. Lett 33, 2347 (2008). [PubMed: 18923618]
11. Pahlevaninezhad H, Lee AMD, Hohert G, Lam S, Shaipanich T, Beaudoin E-L, MacAulay C, Boudoux C, and Lane P, Opt. Lett 41, 3209 (2016). [PubMed: 27420497]
12. Sherlock BE, Phipps JE, Bec J, and Marcu L, Opt. Lett 42, 3753 (2017). [PubMed: 28957119]
13. Presby HM, Appl. Opt 20, 701 (1981). [PubMed: 20309181]
14. Ibrahim A, Devaux B, Habert R, Poulon F, Kudlinski A, Abi Haidar D, Varlet P, Melouki F, and Zanello M, Opt. Lett 41, 5214 (2016). [PubMed: 27842096]
15. Liu J, Sun Y, Qi J, and Marcu L, Phys. Med. Biol 57, 843 (2012). [PubMed: 22290334]
16. Ma D, Bec J, Gorpas D, Yankelevich D, and Marcu L, Biomed. Opt. Express 6, 987 (2015). [PubMed: 25798320]
17. Sherlock BE, Harvestine JN, Mitra D, Haudenschild A, Hu J, Athanasiou KA, Leach JK, and Marcu L, J. Biomed. Opt 23, 1 (2018).
18. Jones G, Jackson WR, and Halpern AM, Chem. Phys. Lett 72, 391 (1980).
19. Magde D, Rojas GE, and Seybold PG, Photochem. Photobiol 70, 737 (1999).
20. Alfonso-Garcia A, Shklover J, Sherlock BE, Panitch A, Griffiths LG, and Marcu L, J. Biophotonics 11, e201700391 (2018). [PubMed: 29781171]

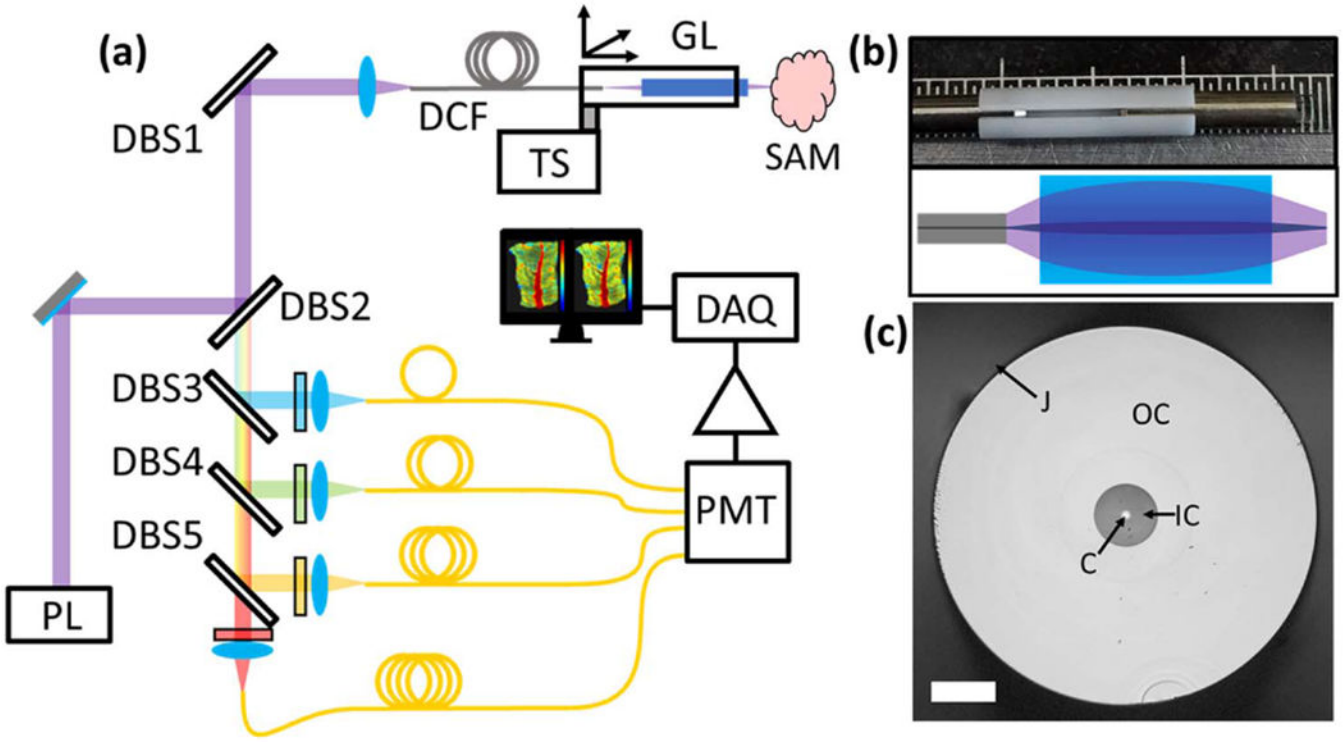

Fig. 1.

(a) Fiber-based multiscale multispectral apparatus schematic. DAQ, data acquisition card; DBS1–DBS5, dichroic beam splitters 1–5; DCF, double-clad fiber; GL, GRIN lens; PL, 355 nm pulsed laser; PMT, photomultiplier tube; SAM, Sample; TS, translation stage. (b) Photograph and schematic diagram of the GRIN lens fiber probe. (c) High-resolution image of the DCF end face. The core (C), inner cladding (IC), pure silica outer cladding (OC), and low-index polymer jacket (J) are all visible. Scale bar, 100 μm.

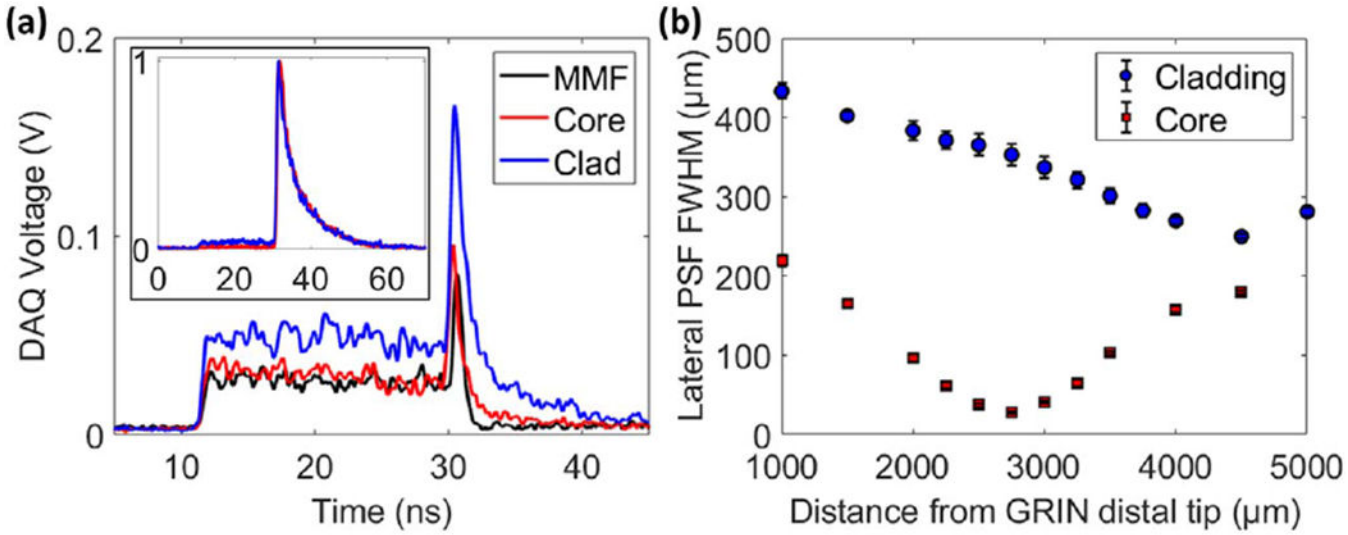

Fig. 2.

(a) Time-resolved fluorescence intensity traces recorded in CH1 for a MMF, DCF core, or DCF cladding guidance of UV fluorescence excitation in the absence of a sample. Inset: normalized DCF core and cladding traces when illuminating a section of murine bone. (b) Lateral PSF FWHM of the DCF core and cladding, measured as a function of distance from the GRIN lens distal tip. The measurements were extracted from the Gaussian fitting to the fluorescence profile recorded when scanning across a 13 µm tungsten wire coated in fluorescent dye.

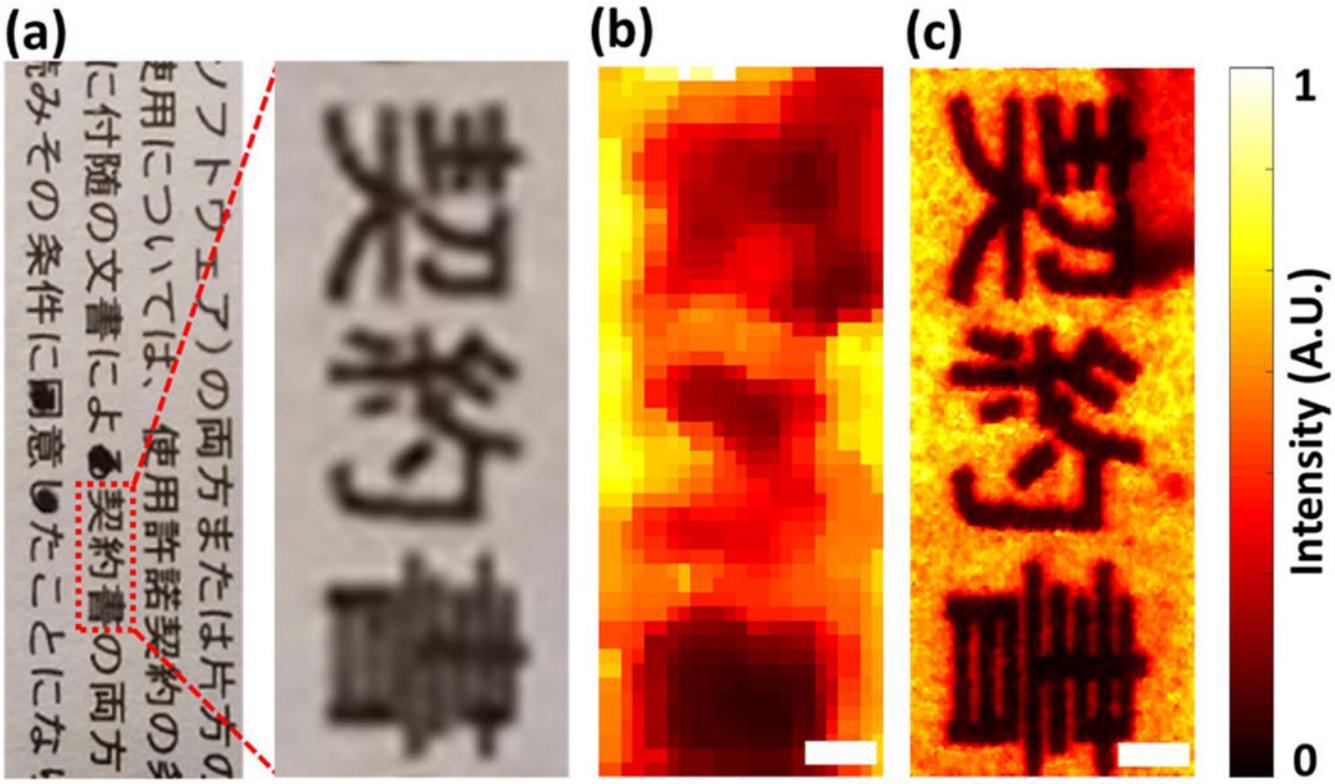

Fig. 3.

(a) Photograph of laser-printed characters on white paper. Fluorescence intensity image of printed characters acquired in CH2 using (b) cladding and (c) core illumination. Scale bar, 500 μm.

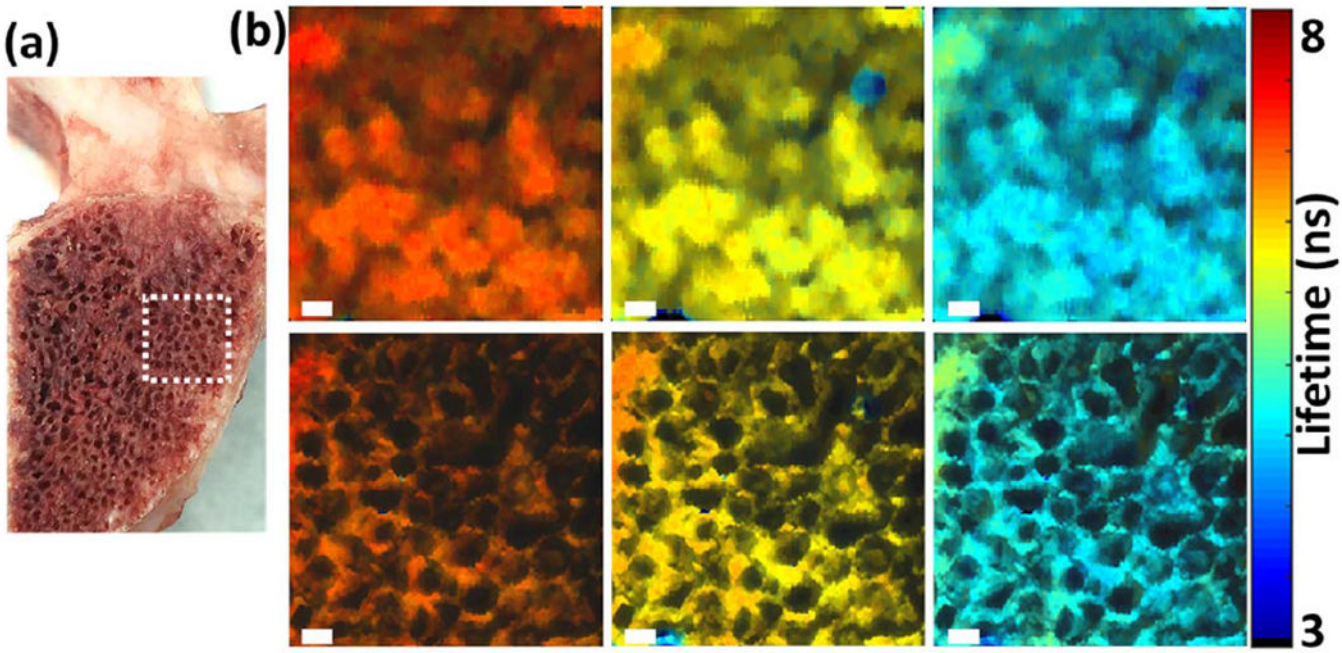

Fig. 4.

(a) Photograph of murine bone. Dashed outline shows the region imaged using a multiscale multispectral fluorescence lifetime system. (b) Intensity-weighted fluorescence lifetime images acquired in (from left to right) CH1, CH2, and CH3. The top (bottom) row shows images of the same field of view acquired using cladding (core) illumination. Scale bar, 500 μm.

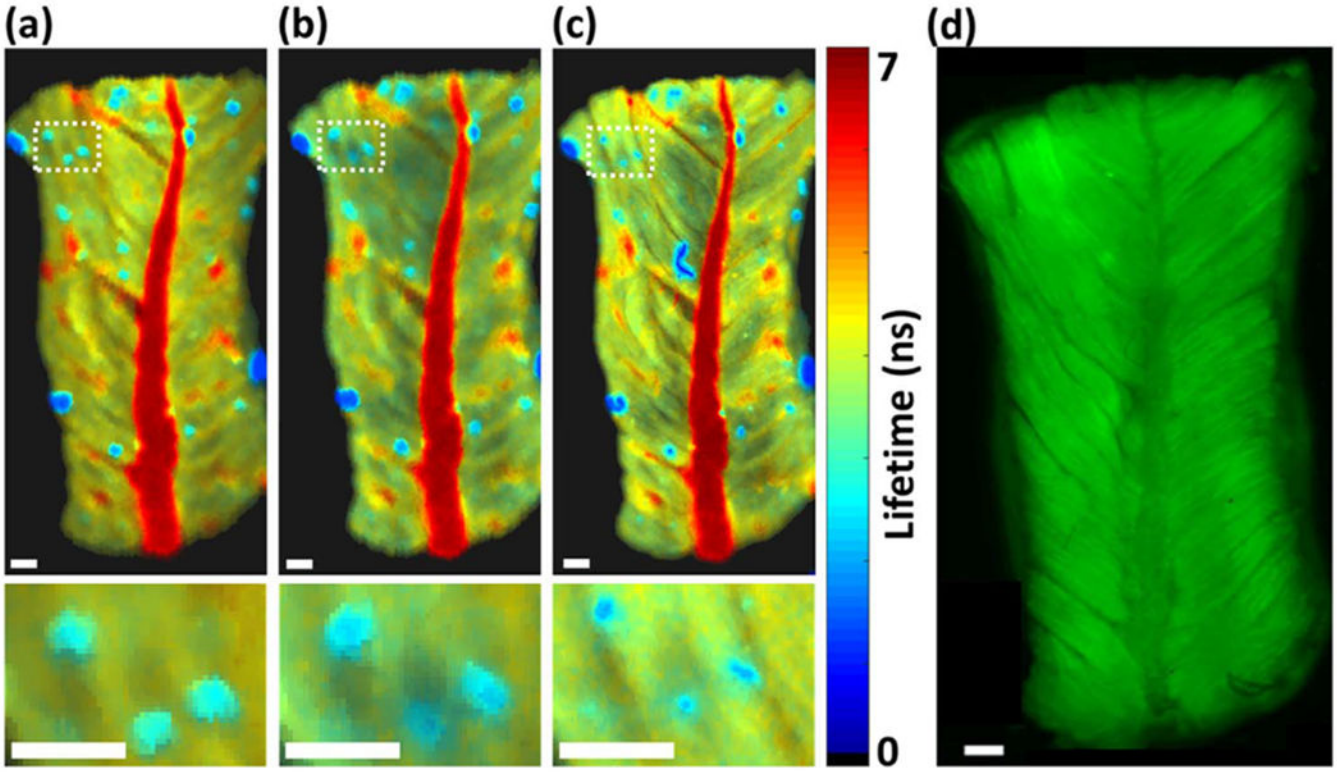

Fig. 5.

(Top row): intensity-weighted fluorescence lifetime images acquired in CH2 of the bovine muscle sample using a (a) MMF, (b) DCF cladding, and (c) DCF core illumination. (Bottom row): zoomed-in images of regions enclosed by a white dashed rectangle. (d) Microscope image of muscle autofluorescence. Scale bar, 1 mm.

Table 1.

Fluorescence Lifetimes of Rhodamine B and Coumarin 1 (in EtOH), Recorded Using a 355 nm Fluorescence Excitation Guided by the DCF Core, DCF Cladding, and a MMF

	Coumarin 1 (EtOH)	Rhodamine B (EtOH)
Fiber	**CH2 Lifetime (ns)**	**CH4 Lifetime (ns)**
DCF core	3.08 ± 0.02	2.72 ± 0.06
DCF cladding	3.08 ± 0.09	2.69 ± 0.08
MMF core	3.00 ± 0.08	2.70 ± 0.03